

Improved reconstruction algorithm for luminescence optical tomography when background lumiphore is present

J. Chang, H. L. Graber, and R. L. Barbour

We examine the impact of background lumiphore on image quality in luminescence optical tomography. A modification of a previously described algorithm [J. Chang, H. L. Graber, and R. L. Barbour, *J. Opt. Soc. Am. A* **14**, 288–299 (1997); J. Chang, H. L. Graber, and R. L. Barbour, *IEEE Trans. Biomed. Eng.* **44**, 810–822 (1997)] that estimates the background luminescence directly from the detector readings is developed. Numerical simulations were performed to calculate the diffusion-regime limiting form of forward-problem solutions for a specific test medium. We performed image reconstructions with and without white noise added to the detector readings, using both the original and the improved versions of the algorithm. The results indicate that the original version produces unsatisfactory reconstructions when background lumiphore is present, whereas the improved algorithm yields qualitatively better images, especially for small target-to-background luminescence yield ratios. © 1998 Optical Society of America

OCIS codes: 260.3800, 110.6960.

1. Introduction

The use of lumiphore to enhance image quality in optical diffusion tomography has been a subject of considerable interest recently.^{1–5} Luminescent compounds play a role in optical tomography analogous to that of radiopharmaceutical agents in nuclear medicine, in that both types of molecules actively emit photons from which projection or tomographic images are reconstructed. In an earlier paper,¹ we described algorithms we developed for reconstruction of two quantities of interest when the background scattering and the absorption coefficients are known. These are the luminescence yield $\gamma\sigma_{a,l}N_0$, where γ is the lumiphore's quantum yield, $\sigma_{a,l}$ is its microscopic absorption cross section, and N_0 is its concentration, and the mean lifetime τ . We showed that $\gamma\sigma_{a,l}N_0$

can be reconstructed from dc (i.e., steady-state, $\omega = 0$) detector readings. If detector readings for at least one $\omega \neq 0$ also are available, then they can, in principle, be used to reconstruct τ directly, without knowledge of $\gamma\sigma_{a,l}N_0$. However, for a numerical reason we adopted a concentration correction that makes use of the $\gamma\sigma_{a,l}N_0$ information during the reconstruction of τ . To implement this correction, one first obtains the maximum value of each $\gamma\sigma_{a,l}N_0$ map, and any value smaller than a threshold fraction of the maximum is set to zero. This modified $\gamma\sigma_{a,l}N_0$ map is then used in the calculation of the weight function (imaging operator) for the corresponding mean lifetime reconstruction. The examples we presented¹ showed that this concentration correction procedure works well in the absence of background lumiphore. Subsequently, however, we have seen that when background lumiphore is present, the reconstruction results are unsatisfactory (see Section 5).

One idea we have pursued in our efforts to deal with the problem just described is to make better use of *a priori* information, a powerful tool for finding the solutions of ill-conditioned problems,⁶ in our image-reconstruction algorithms. For example, previous studies⁷ have demonstrated that positivity and range constraints can effectively improve image quality. However, great care must be taken to use range constraints properly, or they might not provide satisfactory results when background lumiphore is present. Background lumiphore not only significantly increases the detected signal, but also makes it difficult

When this research was performed J. Chang was with the Department of Pathology, State University of New York Health Science Center at Brooklyn, 450 Clarkson Avenue, Brooklyn, New York 11203-2012. J. Chang is currently with the Department of Medical Physics, Memorial Sloan-Kettering Cancer Center, 1275 York Avenue, New York 10021. H. L. Graber and R. L. Barbour are with the Program in Physiology and Biophysics, State University of New York Health Science Center at Brooklyn, 425 Clarkson Avenue, Brooklyn, New York 11203-2012. R. L. Barbour is also with the Department of Pathology.

Received 14 May 1997; revised manuscript received 12 January 1998.

0003-6935/98/163547-06\$15.00/0

© 1998 Optical Society of America

to assign a lower limit to the range constraint. An arbitrary choice of a lower bound (typically zero) is not satisfactory, as shown below in Section 5. Thus a requirement for successful reconstruction by our algorithms is a reasonable estimate of the background lumiphore concentration.

2. Review of Theory and Previous Algorithm

The excitation and the emission light associated with a luminescence process in the frequency domain are governed by a set of coupled radiative transfer equations^{1,2}:

$$\frac{-j\omega\tilde{\phi}_1}{c} + \mathbf{\Omega} \cdot \nabla\tilde{\phi}_1 + (\mu_{T,1} + \mu_{T,1\rightarrow 2})\tilde{\phi}_1 = \tilde{S}_1 + \int_{4\pi} \mu_{s,1}(\mathbf{\Omega}' \cdot \mathbf{\Omega})\tilde{\phi}_1' d\Omega', \quad (1)$$

$$\frac{-j\omega\tilde{\phi}_2}{c} + \mathbf{\Omega} \cdot \nabla\tilde{\phi}_2 + \mu_{T,2}\tilde{\phi}_2 = \tilde{S}_2 + \int_{4\pi} \mu_{s,2}(\mathbf{\Omega}' \cdot \mathbf{\Omega})\tilde{\phi}_2' d\Omega', \quad (2)$$

where the subscripts 1 and 2 denote the excitation and the emitted light, respectively; the \sim symbol denotes the Fourier transform operation; c is the speed of light (cm s^{-1}); ω is the modulation frequency (s^{-1}); $d\Omega$ is the differential solid angle (sr); ϕ_1 and ϕ_2 are the angular intensities ($\text{cm}^{-2} \text{s}^{-1} \text{sr}^{-1}$); \tilde{S}_1 and \tilde{S}_2 are time-harmonic angular source strengths ($\text{cm}^{-3} \text{s}^{-1} \text{sr}^{-1}$); $\mu_s(\mathbf{\Omega}' \cdot \mathbf{\Omega})$ is the macroscopic differential scattering cross section ($\text{cm}^{-1} \text{sr}^{-1}$); μ_T is the macroscopic total cross section (cm^{-1}); and $\mu_{T,1\rightarrow 2}$ (cm^{-1}) is the change in total cross section after the lumiphore is added. Additionally, in the following we make use of the relation $\mu_{T,1\rightarrow 2} = N_g \sigma_{T,1\rightarrow 2}$, where $\sigma_{T,1\rightarrow 2}$ is the microscopic total cross section (cm^2) of the lumiphore and N_g is the concentration (cm^{-3}) of lumiphore in the electronic ground state. It is known from previous studies^{1,2} that $\tilde{S}_2 = \gamma\mu_{T,1\rightarrow 2} \tilde{\phi}_1/[4\pi(1 + j\omega\tau)]$, where $\gamma = \tau/\tau_0$ is the quantum yield (dimensionless), τ_0 is the intrinsic mean lifetime (s) of the luminescent probe's excited state, and $\tilde{\phi}_1 = \int_{4\pi} \phi_1 d\Omega$ is the excitation intensity ($\text{cm}^{-2} \text{s}^{-1}$).

In this study, we consider the case of a single lumiphore in a heterogeneous environment, and work under the assumption that light at the excitation and the emission wavelengths can be detected separately. We assume also (see Section 4) that the lumiphore contributes only a small additional absorption cross section to the medium, so $\sigma_{T,1\rightarrow 2} = \sigma_{a,l}$, and that there is negligible lumiphore saturation, or $N_g \approx N_0$.

In our model $\sigma_{a,l}$ is fixed. As for the mean lifetimes, τ may vary with physiological environment, but τ_0 is fixed. Under these conditions γ cannot be a constant, but it must vary with physiological environment too. In addition, it can be easily shown that the intensity $|\tilde{S}_2| = \gamma\mu_{T,1\rightarrow 2} |\tilde{\phi}_1|/[4\pi(1 + \omega^2\tau^2)^{1/2}]$ is a monotonically increasing function of quantum yield. That is, the intensity of emission light is strongest

when $\gamma = 1$ and gradually decreases with decreasing γ , because of the corresponding increase in the rate of nonradiative de-excitation. Thus to take account of the on-off mechanism introduced by the quantum yield, we use the background-to-target yield ratio [i.e., $(\gamma N_0)_b/(\gamma N_0)_t$] instead of the background-to-target concentration ratio, as our measure of the lumiphore's selectivity for the target region in this study.

Although simultaneous reconstruction of $\gamma\sigma_{a,l}N_0$ and τ from measurements made at a single modulation is possible,³⁻⁵ we have adopted the approach of first reconstructing $\gamma\sigma_{a,l}N_0$ from dc data and subsequently reconstructing τ from ac data. We chose to do this, instead of taking a single-frequency or simultaneous reconstruction approach, on the basis of the results of our previous study on the sensitivity of the detected signal to changes in the properties of the target as a function of modulation frequency.² The method is summarized here (see Refs. 1 and 2 for a more detailed presentation).

A. Steady-State (dc) Source

If we use dc sources, then we have

$$\tilde{R} = \int_V w(\gamma\sigma_{a,l}N_0) d^3r, \quad (3)$$

where \tilde{R} is the detector readings and $w \equiv w_{dc} = \tilde{\phi}_1\tilde{\phi}_2^+/4\pi$ is the weight function, where the $\tilde{\phi}_2^+$ superscript denotes the adjoint. (Here \tilde{R} , $\tilde{\phi}_1$ and $\tilde{\phi}_2^+$ are evaluated at $\omega = 0$.) If $\tilde{\phi}_1$ and $\tilde{\phi}_2^+$ can be precalculated under the assumption that no lumiphore is present, then the unknown quantity $\gamma\sigma_{a,l}N_0$ can be computed by solution of a linear system obtained by discretizing Eq. (3).

B. Time-Harmonic (ac) Source

If modulated sources are used, then we have

$$\tilde{R} = \int_V w \frac{1 - j\omega\tau}{1 + \omega^2\tau^2} d^3r, \quad (4)$$

where $w \equiv w_{ac} = \gamma\sigma_{a,l}N_0\tilde{\phi}_1\tilde{\phi}_2^+/4\pi$. Equation (4) can be discretized, and the real and the imaginary parts of the detector readings give rise to a system of linear equations from which the real part $1/(1 + \omega^2\tau^2)$, the imaginary part $-\omega\tau/(1 + \omega^2\tau^2)$, and their ratio $-\omega\tau$ of the unknown can be reconstructed. Because ω is known, τ can also be deduced.

The implementation of reconstruction involves digitizing the above two equations and solving a system of linear equation using an iterative method (e.g., conjugate gradient descent, projection onto convex sets, or simultaneous algebraic reconstruction technique). Because of the ill-conditioning of the weight function, many kinds of regularization methods are used.^{8,9} In our previous study,⁷ we used positivity constraints, derived from *a priori* knowledge of the target, to regulate the reconstructed results.

3. Algorithm

In this study, a new procedure was developed to improve the reconstruction of luminescence yield and the mean lifetime when background lumiphore is present; we accomplish this by directly estimating the background lumiphore contribution from detector readings. Here we assume that the background lumiphore is uniformly distributed with a constant concentration and mean lifetime and that the target is an isolated object. Under these assumptions, the new procedure is

1. Estimate the background luminescence yield (BLY) by means of the maximum possible yield principle (MPYP). This is a technique to compute a reasonable estimate bly of the (true) BLY from the dc detector readings. Suppose that all of the detected signal comes from background lumiphore. Since the BLY is constant, it is equal to the ratio of a detector reading to the corresponding weight function integrated over the entire volume of the medium. An estimate of BLY is obtained from each detector reading, and the lowest of these estimates is used as bly . BLY must be $\leq bly$, since $BLY > bly$ would imply a negative contribution to the detector readings from the target.

2. Reconstruct $\gamma\sigma_{a,l}N_0$ with an iterative algorithm with a range constraint, where the upper and the lower bounds are the maximum possible target luminescence yield and bly . The former is estimated by choosing a number ~ 10 times greater than bly divided by the expected background-to-target yield ratio, which can be estimated on the basis of previous experience and on the known properties of the dye.

3. Restrict the target volume by setting $\gamma\sigma_{a,l}N_0$ to bly in all voxels where $\gamma\sigma_{a,l}N_0 - bly$ is less than a preset fraction of $\max(\gamma\sigma_{a,l}N_0) - bly$.

4. Reconstruct the mean lifetime of the target and the background. Here we sum the weight function over all the background voxels, so that the unknowns in the reconstruction are the voxels in the target plus one lumped background voxel, thereby greatly reducing the dimension of the vector of unknowns.

4. Method

Numerical simulations were performed to calculate solutions to the diffusion equations describing the excitation and the emission fields.^{1,2} The phantom was an infinite medium with background lumiphore uniformly distributed in an $8.0\text{ cm} \times 8.0\text{ cm} \times 0.1\text{ cm}$ square region of interest (ROI) [Fig. 1(A)]. This area is discretized into $0.25\text{ cm} \times 0.25\text{ cm} \times 0.1\text{ cm}$ square voxels. The target was a smaller square located at one of two locations—the center of the ROI [Fig. 1(B)] or halfway between the center and the bottom edge of the ROI [Fig. 1(C)]. In each target position, four test cases corresponding to different target sizes were studied: $0.5\text{ cm} \times 0.5\text{ cm} \times 0.1\text{ cm}$, $1.0\text{ cm} \times 1.0\text{ cm} \times 0.1\text{ cm}$, $1.5\text{ cm} \times 1.5\text{ cm} \times 0.1\text{ cm}$, and $2.0\text{ cm} \times 2.0\text{ cm} \times 0.1\text{ cm}$. The macroscopic cross sections at both excitation and emis-

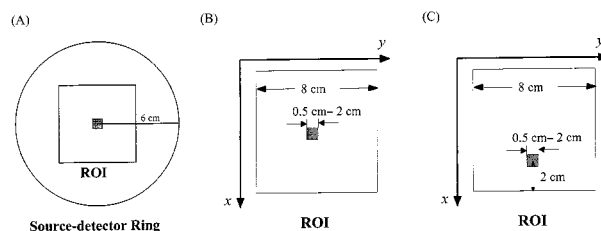


Fig. 1. (A) Source–detector ring and phantom structure used for diffusion computations. Two target positions were adopted in this study. They are (B) the center of the ROI, and (C) the midway point between the center of ROI and its bottom edge. Four different target sizes were studied for each position, ranging from a $0.5\text{ cm} \times 0.5\text{ cm}$ square to a $2.0\text{ cm} \times 2.0\text{ cm}$ square. The thickness of the ROI is 1 mm. Thus it is essentially a 2D region, although 3D diffusion model is used for the computations.

sion wavelength were $\mu_s = 1000\text{ m}^{-1}$ and $\mu_a = 3\text{ m}^{-1}$. The additional absorption cross section introduced by the lumiphore was $\mu_{a,l} = 0.01\text{ m}^{-1}$. The intrinsic mean lifetime of lumiphore in both the background and the target portions of the ROI was $\tau_0 = 5 \times 10^{-9}\text{ s}$ in every computation. The quantum yields in the background and the target were $\gamma_t = 1$, $\gamma_b = 0.2$ for the centered targets, and $\gamma_t = 0.2$, $\gamma_b = 1$ for the off-center targets. Diffusion equation solutions were computed for dc illumination and for time-harmonic illumination at a modulation frequency of 100 MHz. These computations supplied the required information for reconstructions of luminescence yield and of mean lifetime. Different levels of Gaussian noise (where noise level is defined as the ratio of the signal mean to the noise standard deviation) were also added to the detector readings.

The goal of reconstruction is to recover the product of the lumiphore's quantum yield and absorption coefficient $\gamma\sigma_{a,l}N_0$ and its mean lifetime τ from the simulated detector readings, with or without added noise. We obtained images by using both the previously described¹ and the improved versions of the reconstruction algorithm with the CGD method, both of which were terminated after 10,000 iterations. The thickness of the ROI is 1 mm. Thus the problems studied here are essentially two dimensional (2D), although a three-dimensional (3D) diffusion model was used for the simulations. A 2D model rather than a 3D one was chosen for this study simply for the purpose of reducing the computation time. It is fully understood that a 2D reconstruction is easier than a 3D one would be, as the difficulty index (i.e., the ratio of the concentration–volume product of the background to that of the target) described in our previous study¹⁰ goes as the second and the third power of the linear dimension in the 2D and the 3D cases, respectively.

5. Results

Figure 2 shows the reconstructed $\gamma\sigma_{a,l}N_0$ and τ for different target sizes when the background-to-target $\gamma\sigma_{a,l}N_0$ ratio is 0.01 and when the previously described algorithm with a positivity constraint on

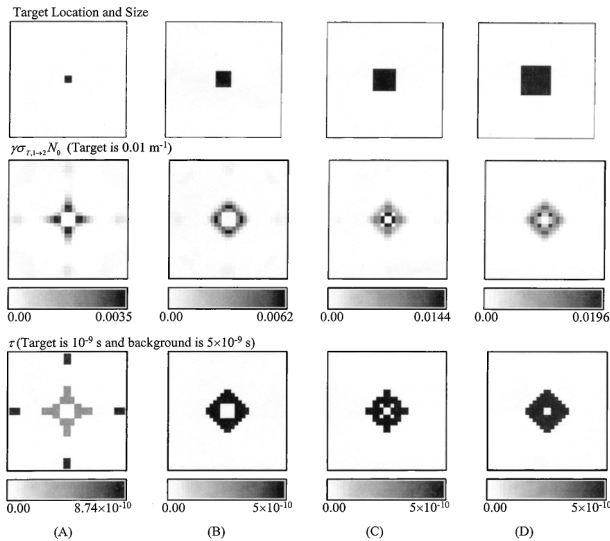


Fig. 2. Reconstructions of luminescence yield $\gamma\sigma_{a,l}N_0$ and mean lifetime τ with background-to-target $\gamma\sigma_{a,l}N_0$ ratio of 0.01 and different target sizes, (A) 0.5 cm \times 0.5 cm \times 0.1 cm, (B) 1.0 cm \times 1.0 cm \times 0.1 cm, (C) 1.5 cm \times 1.5 cm \times 0.1 cm, and (D) 2.0 cm \times 2.0 cm \times 0.1 cm, and with the previously described algorithm^{1,2} with positivity constraints.

$\gamma\sigma_{a,l}N_0$ and a 5×10^{-10} s to 5×10^{-9} s range constraint on τ is used. (A) 0.5 cm \times 0.5 cm \times 0.1 cm, (B) 1.0 cm \times 1.0 cm \times 0.1 cm, (C) 1.5 cm \times 1.5 cm \times 0.1 cm, and (D) 2.0 cm \times 2.0 cm \times 0.1 cm. Figure 3 shows the reconstruction results for targets of different sizes when the background-to-target $\gamma\sigma_{a,l}N_0$ ratio was 0.2 and when the improved algorithm was used instead. The $\gamma\sigma_{a,l}N_0$ product was constrained to lie between the maximum target value (0.05 m^{-1}) and the *bly* selected by the algorithm. Figure 4 demonstrates the reconstruction results for the off-centered case in which the target sizes, background-to-target $\gamma\sigma_{a,l}N_0$ ratio, and reconstruction algorithm

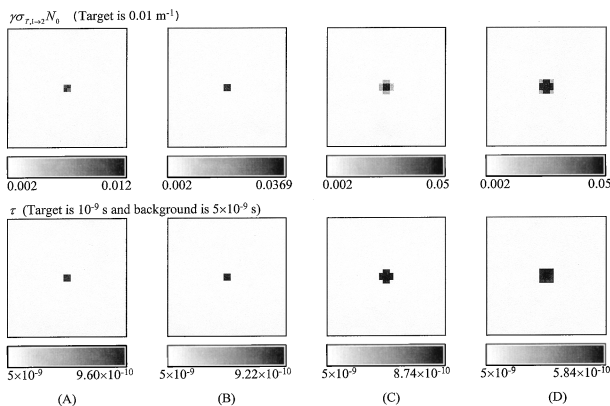


Fig. 3. Reconstruction results with background-to-target $\gamma\sigma_{a,l}N_0$ ratio of 0.2 and different target sizes, when the improved algorithm with range constraints is used. Target locations and sizes are the same as for Fig. 2, but background-to-target $\gamma\sigma_{a,l}N_0$ ratio is 20 times larger in these cases. Note that the gray scale of the τ is reversed for display purposes. That is, the darker region corresponds to lower values.

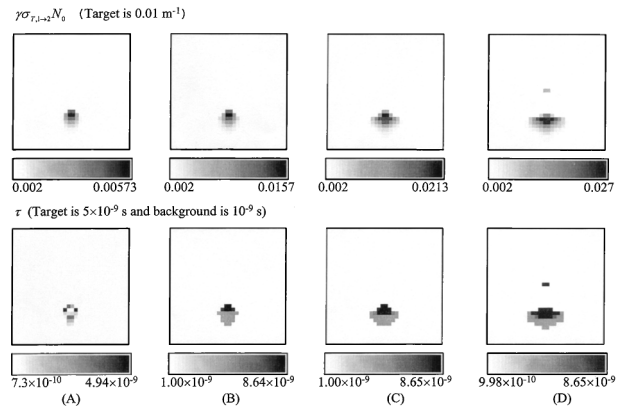


Fig. 4. Reconstruction results of the off-center case with background-to-target $\gamma\sigma_{a,l}N_0$ ratio of 0.2 and different target sizes when the improved algorithm with range constraints is used. Centers of targets are located halfway between the center and the bottom edge of the ROI. Sizes are the same as for Fig. 2, but the background-to-target $\gamma\sigma_{a,l}N_0$ ratio is 20 times larger in these cases. Notice that the numerical values of τ can exceed the maximum value of the constraint range because they are the ratios of the reconstructed real and imaginary parts of the unknown quantities in Eq. (4). If range constraints are applied directly to the above reconstructed τ , the numerical values of the target and the background mean lifetimes are within 2.0% of the correct values.

are the same as in Fig. 3. The previously described algorithm, when applied to the same data as used to produce Fig. 4, gave results (not shown) in which neither the qualitative (location, size, shape) nor the quantitative aspects were correct. A comparison of reconstructed $\gamma\sigma_{a,l}N_0$ when the previous and the improved algorithms with background-to-target $\gamma\sigma_{a,l}N_0$ ratio of 0.01 were used is shown in Fig. 5. The target size is 1.0 cm \times 1.0 cm \times 0.1 cm. In Fig. 6 we show the images reconstructed by improved algorithm with constraints for a fixed background-to-target yield ratio of 0.01 and a fixed target size of 2.0 cm \times

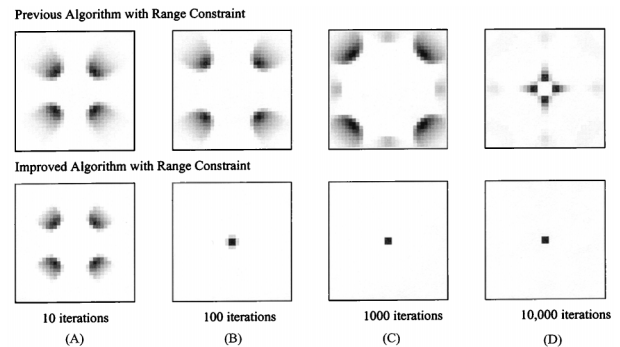


Fig. 5. Comparison of images reconstructed by use of the previous and the improved algorithms, with background-to-target $\gamma\sigma_{a,l}N_0$ ratio of 0.01 after (A) 10 iterations, (B) 100 iterations, (C) 1000 iterations, and (D) 10,000 iterations. A four-lobed pattern was observed in both cases after 10 iterations. As the number of iterations increases, the improved algorithm accurately reconstructs the target's size and position, whereas the results from the previous algorithm still contain unacceptable artifacts.

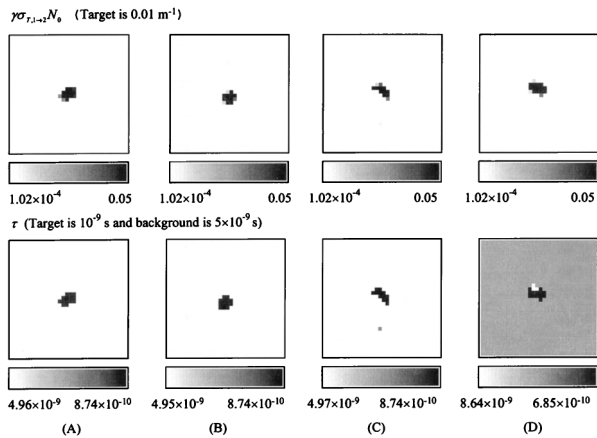


Fig. 6. Reconstruction results of the center case with a background-to-target $\gamma\sigma_{a,l}N_0$ ratio of 0.01 and different levels of added noise, with target size $2.0 \text{ cm} \times 2.0 \text{ cm} \times 0.1 \text{ cm}$, and when the improved algorithm with range constraints is used. (A) 1.0%, (B) 3.0%, (C) 5.0%, and (D) 10.0% noise.

$2.0 \text{ cm} \times 0.1 \text{ cm}$, with different levels of added noise (1.0%, 3.0%, 5.0%, and 10.0%).

6. Discussion

Our earlier reports^{1,2} described an algorithm that sequentially computes $\gamma\sigma_{a,l}N_0$ and τ when dc and ac data are used. (Although neither sequential computation nor the use of different ω 's is essential,^{3,4} we based our choice of these conditions on the different ω dependence of detector sensitivity to changes in the quantities we reconstruct.² In the presence of background lumiphore, however, the original algorithm failed to provide accurate quantitative results for either $\gamma\sigma_{a,l}N_0$ or τ (Fig. 2), even when a positivity constraint was used. The algorithm set many voxels to zero while reconstructing $\gamma\sigma_{a,l}N_0$ instead of generating the uniform background we expected. It is likely that this is a consequence of the underdeterminedness of the weight matrix, which has infinitely many left inverses, and of a uniform distribution not lying on the fastest-converging path chosen by the algorithm. In addition, the degradation of image quality is a function of target size. That is, for a fixed background-to-target yield ratio, more accurate reconstructions were obtained for larger targets. This indicates that the background-to-target yield ratio is not by itself a meaningful index of the difficulty of an image reconstruction problem and that the target size should be considered as well.

The reconstructions shown in Figs. 3 and 4, produced by the revised algorithm, show significant improvement over those obtained from the original version, even though the background-to-target yield ratio is 20 times larger in Figs. 3 and 4 than in Fig. 2. The correlation of image quality with target size is not significant, or even becomes negative, because a more accurate estimate of the BLY is obtained when the MPYP is used than when zero is taken for the lower bound. The size of the target, however, is underestimated for larger targets [Figs. 3(B)–3(D)],

whereas $\gamma\sigma_{a,l}N_0$ is quantitatively overestimated. This is probably a consequence of the underdeterminedness of the weight matrix, and one can reduce the error by using regularization techniques.^{8,9} In addition, the reconstructed mean lifetime is less accurate for larger objects because of the underestimated target size.

The overestimate of $\gamma\sigma_{a,l}N_0$ and the underestimate of the target size is less significant in Fig. 4 because the target is closer to the detector ring and the weight matrix is better conditioned. Note that the range constraints in the mean lifetime reconstruction are applied to the real and the imaginary parts of Eq. (4), not to their ratio. Thus the reconstructed mean lifetime may lie outside the constraint range, as is seen in Figure 4. If the range constraint was also applied to the ratio, the reconstructed mean lifetime is within 2% of the correct values in the mean lifetime reconstruction of Fig. 4. The negative correlation between image quality and target size seems reasonable when we recall that the presence of a large target increases the detector readings appreciably above that due to the background. Thus the BLY is overestimated by an amount depending on the target's yield, size, and location. High target yields, large targets, and targets located near sources or detectors result in significant overestimates of the BLY, thus distorting the reconstructed images.

The images reconstructed from background-dominant signals did not show a uniform distribution of the background lumiphore but a four-lobed pattern (Fig. 5), which is a consequence of the underdeterminedness of the inverse problem and the ill-conditioning of the weight matrix. (The exact number and shapes of the lobes is case dependent. Four symmetric lobes were obtained here because the phantom consists of a square target in a square ROI, both centered in the source–detector ring, and the background medium is homogeneous.) Unlike the effect of noise, the influence of which is distributed throughout the reconstruction (Fig. 6 and Ref. 11), this pattern was observed in early iterations and may or may not improve after more iterations, depending on which algorithm was used. This poses a problem for image reconstruction when background lumiphore is present, because it prevents us from using early reconstruction results, which is an advantage of an iterative algorithm. The addition of noise distorted the reconstructed images in a noise-level-dependent manner. Results shown in Fig. 6 demonstrate that reasonable qualitative accuracy was obtained from the improved algorithm even for 10% Gaussian noise added to the detector readings. The quantitative estimate of $\gamma\sigma_{a,l}N_0$ is inaccurate because of the noise. The mean lifetime values, however, are acceptable for as much as 5% noise, even if the quantitative estimate of $\gamma\sigma_{a,l}N_0$ is incorrect. This is reasonable because $\gamma\sigma_{a,l}N_0$ is used only to delineate the target from the background. Its quantitative value is not important, because it is factored out in the mean lifetime reconstruction when the ratio of imaginary to real parts is computed.

The improved algorithm works well for uniformly distributed background lumiphore and one isolated target, as demonstrated in this paper. What about more complicated objects, with nonuniform background lumiphore and multiple targets? First, the MPYP is always a useful tool to make a reasonable estimate of the lower bound for the range constraints and is definitely better than blindly setting the lower bound to zero. For multiple or larger targets in which cases *bly* may be a poor estimate of BLY, an iterative update of the maximum possible yield may be used to remove the influence of the targets. That is, after reconstructing the targets from the initial *bly*, one can compute a new *bly* by subtracting the contribution of the initial reconstructed target from the detector readings for use in the next reconstruction. In addition, it was assumed in this study that the absorption coefficient introduced by the lumiphore is much smaller than the absorption cross section of the tissue, so that a one-step perturbation approach is sufficient for accurate image reconstruction. When the lumiphore contributes a significant fraction of the medium's overall absorption cross section, an iterative update scheme¹²⁻¹⁴ should be used. In either case, the improved algorithm described here should be used if range constraints are applied. That is, the ratio of the detector readings to the weight function provides an accurate estimate of BLY when one assumes the updated weight function is accurate.

We acknowledge support from NIH grant RO1-CA59955 and RO1-CA66184-02.

References

1. J. Chang, H. L. Graber, and R. L. Barbour, "Luminescence optical tomography of dense scattering media," *J. Opt. Soc. Am. A* **14**, 288-299 (1997).
2. J. Chang, H. L. Graber, and R. L. Barbour, "Imaging of fluorescence in highly scattering media," *IEEE Trans. Biomed. Eng.* **44**, 810-822 (1997).
3. D. Y. Paithankar, A. U. Chen, B. W. Pogue, M. S. Patterson, and E. M. Sevick-Muraca, "Fluorescence lifetime imaging with frequency-domain photon migration measurement," *Appl. Opt.* **36**, 2260-2272 (1997).
4. M. A. O'Leary, D. A. Boas, X. D. Li, B. Chance, and A. G. Yodh, "Fluorescence lifetime imaging in turbid media," *Opt. Lett.* **21**, 158-160 (1996).
5. J. Wu, Y. Wang, L. Perelman, I. Itzkan, R. R. Dasari, and M. S. Feld, "Analytical model for extracting intrinsic fluorescence in turbid media," *Appl. Opt.* **32**, 3585-3595 (1993).
6. D. C. Youla, "Mathematical theory of image reconstruction by the method of convex projections," in *Image Recovery: Theory and Application*, H. Stark, ed. (Academic, New York, 1987).
7. J. Chang, H. Graber, R. L. Barbour, and R. Aronson, "Recovery of optical cross-section perturbations in dense scattering media by transport-theory-based imaging operators and steady-state simulated data," *Appl. Opt.* **35**, 3963-3978 (1996).
8. S. R. Arridge, "Forward and inverse problems in time-resolved infrared imaging," in *Medical Optical Tomography: Functional Imaging and Monitoring*, G. J. Mueller, B. Chance, R. R. Alfano, S. R. Arridge, J. Beuthan, E. Gratton, M. Kaschke, B. Masters, S. Svanberg, and P. van der Zee, eds., Vol. IS11 of SPIE Institute Series (SPIE Press, Bellingham, Wash., 1993), pp. 35-64.
9. J. Chang, W. Zhu, Y. Wang, H. L. Graber, and R. L. Barbour, "A regularized progressive expansion algorithm for recovery of scattering media from time-resolved data," *J. Opt. Soc. Am. A* **14**, 306-312 (1997).
10. J. Chang, H. L. Graber, and R. L. Barbour, "Concentration, size, mean lifetime, and noise effects on image quality in luminescence optical tomography," in *Optical Tomography and Spectroscopy of Tissue: Theory, Instrumentation, Model, and Human Studies*, B. Chance and R. R. Alfano, eds., *Proc. SPIE* **2979**, 750-758 (1997).
11. J. Chang, H. L. Graber, and R. L. Barbour, "Dependence of optical diffusion tomography image quality on image operator and noise," in *Proceedings of 1995 IEEE Medical Imaging Conference*, (Institute of Electrical and Electronics Engineers, New York, 1995), pp. 1524-1528.
12. Y. Yao, Y. Wang, Y. Pei, W. Zhu, and R. L. Barbour, "Frequency-domain optical imaging of absorption and scattering distributions by a Born iterative method," *J. Opt. Soc. Am. A* **14**, 325-342 (1997).
13. B. W. Bogue, M. S. Patterson, H. Jiang, and K. D. Paulsen, "Initial assessment of a simple system for frequency domain diffuse optical tomography," *Phys. Med. Biol.* **40**, 1709-1729 (1995).
14. M. Schweiger, S. R. Arridge, and D. T. Delpy, "Application of the finite-element method for the forward and inverse models in optical tomography," *J. Math. Imaging Vision* **13**, 263-283 (1996).